

# RECONFIGURATION MANEUVERS FOR SWARMS OF HIGH AREA-TO-MASS RATIO SPACECRAFT

Giorgio Mingotti<sup>(1)</sup> and Colin McInnes<sup>(2)</sup>

<sup>(1)(2)</sup>*Advanced Space Concepts Laboratory, Department of Mechanical & Aerospace Engineering,  
University of Strathclyde, 75 Montrose Street, G1 1XJ Glasgow, United Kingdom.  
e-mail: giorgio.mingotti@strath.ac.uk, colin.mcinnnes@strath.ac.uk*

**Abstract:** *Reconfiguration maneuvers and maintenance strategies for formation-flying are investigated in this paper, where femto-spacecraft with high area-to-mass ratio and small length-scale are considered. Assuming the exact  $J_2$  nonlinear relative dynamics, an optimal control problem is formulated to accomplish the maneuvers. A continuous control acceleration is applied to the system dynamics via a propellant-free approach, which exploits differential solar radiation pressure by means of electrochromic coating. Different control authorities are considered: femto-spacecraft with full and limited control capability are investigated. Thanks to the advances in miniaturised technology, a great number of electromechanical devices can be manufactured and deployed at low cost with active sensors on-board. A new class of space missions is enabled, based on swarms of micro-spacecraft with sensing, computing, bi-directional communicating and micro-power sources.*

**Keywords:** *Relative Motion, Solar Radiation Pressure, Femto-Spacecraft, Electrochromic Control.*

## 1. Introduction

The recent developments in spacecraft design exploiting miniaturised electromechanical systems with sensing, computing, bi-directional communicating and micro-power functions have enabled a new class of low-cost, low-weight micro-scale spacecraft suitable for use in swarm applications. Current concepts for functional devices in space have been designed by exploiting existing capability, such as satellite-on-a-chip [1]. Distributed devices for Earth observation and communication, autonomous on-orbit self-assembly, diagnostic or environmental detection in the proximity of a large satellite are among the prospective missions that may be enabled. The concept of a swarm of separated elements cooperating coherently enables, for example, the implementation of extremely large aperture radio frequency or optical antennae. These elements would be free-flying in space, either controlled by active or natural forces for each element to stay within a prescribed volume.

The last few decades have seen a growing interest in space missions for remote sensing of the Earth. Numerous missions carrying active and passive sensors for military and civil applications have been implemented. Different kinds of sensors are currently available to obtain a complete set of information useful for a plethora of applications (i.e., atmospheric gas monitoring, landslide control, polar ice monitoring, harbour monitoring, etc.). However, due to the high overall system complexity of space missions, the raw data products can only be obtained at a relatively high cost. This reduces the diffusion and the exploitation of such raw data, especially for civil applications, where Earth-based solutions often result to be cheaper (i.e., terrestrial monitoring of the environ-

ment). The aim of this paper is to propose a novel concept for cost effective space missions in order to make remote sensed data accessible to a broader user community.

Reconfiguration maneuvers for relative motion are investigated in this work, assuming High Area-to-Mass Ratio (HAMR) femto-spacecraft. Considering the exact  $J_2$  nonlinear relative dynamics, an optimal control problem is formulated to accomplish the maneuvers. A continuous control acceleration is applied to the system orbital- and attitude- dynamics via a propellant-free approach, which exploits differential solar radiation pressure by means of electrochromic coating. Thanks to the advances in miniaturised technology, a great number of electromechanical devices can be manufactured and deployed at low cost with active sensors on-board.

The exploitation of orbital dynamics at small-length scale and so high area-to-mass ratio requires entirely new techniques for modelling and relative motion control. Solar radiation pressure and aerodynamic drag may become dominant with respect to the Earth's gravity [2]. Assuming the femto-devices are coated with an electrochromic material, the relative motion within the swarm is continuously controlled via the modulation of differential solar radiation pressure  $dc_{rasrp}$ : the optical properties of the elements change when an electrical current is applied [3]. A propellant-free control method is developed to design and maintain the relative orbits of the swarm. The dynamics is initially based on the linearised formulation of the relative motion of - for a sake of clarity - only two femto-spacecraft flying in close proximity, assuming they are in low, circular orbits around a spherical Earth. Then the dynamical model is extended to include the perturbation caused by the Earth's oblateness [4] and to consider multiple spacecraft; therefore, the exact nonlinear  $J_2$  relative dynamics for each spacecraft is assumed. Moreover, femto-spacecraft with full and limited control capability are investigated.

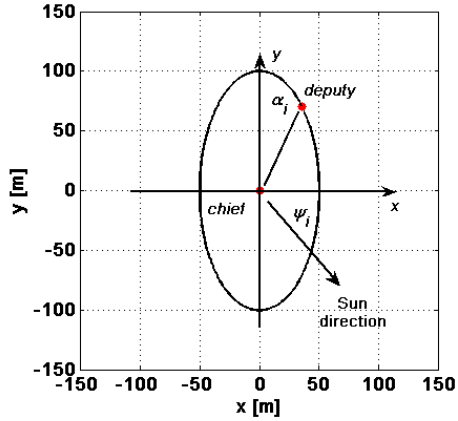
This paper is divided into five main Sections: *Linear Dynamics*, *Nonlinear Dynamics*, *Controlled Dynamics*, *Optimal Control Problem* and *Test Cases*.

In Section *Linear Dynamics*, the linearized relative dynamics of the high area-to-mass ratio and small length scale spacecraft is introduced. Then the exact nonlinear dynamics including the Earth oblateness is discussed in Section *Nonlinear Dynamics*. This is followed by Section *Controlled Dynamics*, where the control capability of the swarm of femto-spacecraft are described. Later on, in Section *Optimal Control Problem*, the optimization formalism is introduced, while in Section *Test Cases*, the test cases are presented. At the end, in *Conclusion*, the final remarks are discussed.

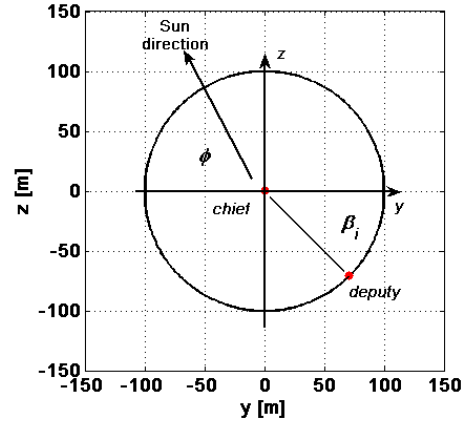
## 2. Linear Dynamics

This section introduces the basics to describe the barycentric motion of multiple *micro*-spacecraft. For a sake of clarity in the following formulation, the relative motion dynamics of two femto-spacecraft in close proximity, named *chief* and *deputy* respectively, traveling around a spherical Earth is considered. It is assumed that the chief flies on a circular low-Earth orbit.

Assuming that the orbital radius of the chief spacecraft is much greater than the relative distance between the spacecraft and considering the *Satellite Coordinate System* (RSW), the linearized relative motion dynamics can be written in the form of the *Clohessy-Wiltshire* or *Hill's* (CWH)



(a) Projected Circular Orbit (PCO) in the  $x - y$  plane view. The parameter  $\alpha_i$  stands for the position of the deputy spacecraft along the periodic orbit, while the parameter  $\psi_i$  stands for the *in-plane* Sun-direction with respect to the chief spacecraft reference frame.



(b) Projected Circular Orbit (PCO) in the  $y - z$  plane view. The parameter  $\beta_i$  stands for the position of the deputy spacecraft along the periodic orbit, while the parameter  $\phi$  stands for the *out-of-plane* Sun-direction with respect to the chief spacecraft reference frame.

**Figure 1. Relative motion parameters and Sun-direction geometry.**

equations [5]:

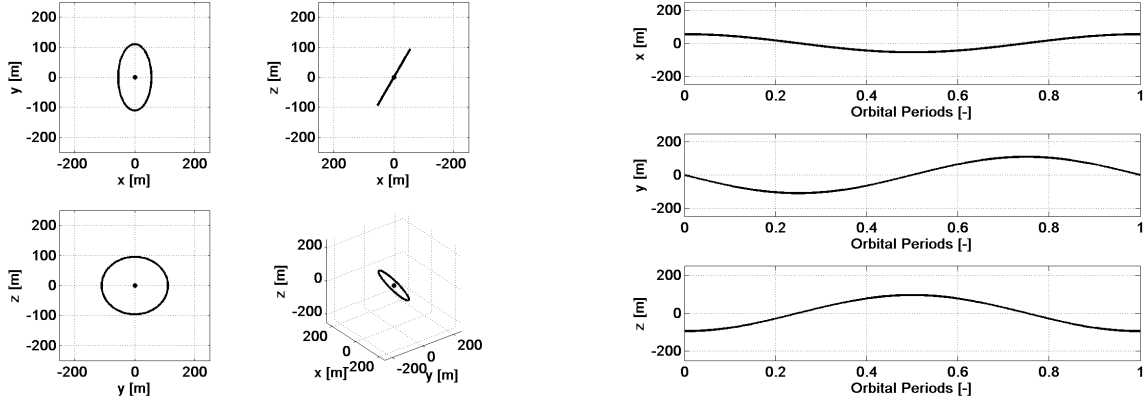
$$\begin{aligned}
 \ddot{x} - 2\omega_n \dot{y} - 3\omega_n^2 x &= a_x \\
 \ddot{y} + 2\omega_n \dot{x} &= a_y \\
 \ddot{z} + \omega_n^2 z &= a_z
 \end{aligned} \tag{1}$$

The system of equations written above, when the accelerations  $a_x = a_y = a_z = 0$ , has an analytic solution of the following form:

$$\begin{aligned}
 x(t) &= 4x_i + \frac{2\dot{y}_i}{\omega_n} + \frac{\dot{x}_i}{\omega_n} \sin(\omega_n t) - \left(3x_i + \frac{2\dot{y}_i}{\omega_n}\right) \cos(\omega_n t) \\
 y(t) &= y_i + \frac{2\dot{x}_i}{\omega_n} + \frac{2\dot{x}_i}{\omega_n} \cos(\omega_n t) + \left(6x_i + \frac{4\dot{y}_i}{\omega_n}\right) \sin(\omega_n t) - (6\omega_n x_i + 3\dot{y}_i)t \\
 z(t) &= z_i \cos(\omega_n t) + \frac{\dot{z}_i}{\omega_n} \sin(\omega_n t) \\
 \dot{x}(t) &= \frac{\dot{x}_i}{\omega_n} \omega_n \cos(\omega_n t) + \left(3x_i + \frac{2\dot{y}_i}{\omega_n}\right) \omega_n \sin(\omega_n t) \\
 \dot{y}(t) &= 6\omega_n x_i + 3\dot{y}_i - 2\dot{x}_i \sin(\omega_n t) + (6\omega_n x_i + 4\dot{y}_i) \cos(\omega_n t) \\
 \dot{z}(t) &= -z_i \omega_n \sin(\omega_n t) + \dot{z}_i \omega_n \cos(\omega_n t)
 \end{aligned} \tag{2}$$

with given initial conditions  $(x_i, y_i, z_i, \dot{x}_i, \dot{y}_i, \dot{z}_i)$ .

Being interested in bounded motion, the initial conditions are assumed such that the secular term vanishes (i.e., the coefficient multiplying  $t$ ). Recalling that orbits are circular, the angular rate  $\omega_n$



(a) Relative motion configuration, natural dynamics (General Circular Orbit (GCO)).

(b) Relative coordinates evolution, natural dynamics (General Circular Orbit (GCO)).

**Figure 2. Formation-flying relative CWH dynamics.**

is simply the satellite's mean motion:

$$\omega_n = \sqrt{\frac{\mu}{r_{chief}^3}} \quad (3)$$

where  $r_{chief}$  is the radial distance of the chief spacecraft, assuming an orbital altitude of 775 km, and  $\mu$  is the Earth's gravitational constant. The nominal orbital period is therefore  $T_n = 6020.7$  s.

The periodic analytic solutions represented by Eqs. 2 can be re-arranged in a compact fashion [6], and a sample General Circular Orbit (GCO) is presented in Fig. 2:

$$\begin{bmatrix} x(t) \\ y(t) \\ z(t) \\ \dot{x}(t) \\ \dot{y}(t) \\ \dot{z}(t) \end{bmatrix} = \begin{bmatrix} a_i/2 \sin(\omega_n t + \alpha_i) \\ a_i \cos(\omega_n t + \alpha_i) + c_i \\ b_i \sin(\omega_n t + \beta_i) \\ a_i/2 \omega_n \cos(\omega_n t + \alpha_i) \\ -a_i \omega_n \sin(\omega_n t + \alpha_i) \\ b_i \omega_n \cos(\omega_n t + \beta_i) \end{bmatrix} \quad (4)$$

Depending upon the choice of free-parameters  $a_i$ ,  $b_i$ ,  $c_i$ ,  $\alpha_i$  and  $\beta_i$ , relative orbits of various shapes and sizes can be obtained:

- Projected Circular Orbit (PCO) in the  $y - z$  plane (see Fig. 1(b));
- General Circular Orbit (GCO) in three-dimensions;
- Leader Follower Configuration (LFC);
- Ecliptic Planar Orbit (EPO) in the  $x - y$  plane.

The initial parameter  $a_i$  stands for the in-plane  $x - y$  orbit amplitude,  $b_i$  the initial out-of-plane  $z$  orbit amplitude, while  $c_i$  describes the initial location of the center of the formation along the

y axis. Finally, the parameter  $\alpha_i$  describes the initial position of the deputy spacecraft along the periodic orbit around the chief in the  $x - y$  plane (see Fig. 1(a)), while the parameter  $\beta_i$  describes the initial out of plane position of the deputy spacecraft (see Fig. 1(b)).

### 3. Nonlinear Dynamics

The purely central force field of the underlying assumptions of Eqs. 1 makes the analytic solution Eqs. 2 unsuitable to simulate more realistic scenarios. The second degree zonal spherical harmonic of the Earth  $J_2 = 1082 \times 10^{-6}$ , produces the primary disturbing potential due to the Earth's oblateness.

The  $J_2$  generated perturbations include secular, long-periodic, and short-periodic components, which consequently will disturb the satellite orbits, for instance, precession of ascending node  $\dot{\Omega}$ , and drifts in argument of perigee  $\dot{\omega}$  and the mean anomaly  $\delta\dot{M}$ .

Therefore, a more accurate dynamical model is assumed in this study, which includes the  $J_2$  perturbation [4]. Assuming the *Earth Centered Inertial* (ECI) coordinate frame, the position, velocity and angular momentum vectors of the chief spacecraft are  $\mathbf{r}$ ,  $\dot{\mathbf{r}}$  and  $\mathbf{h} = \mathbf{r} \times \dot{\mathbf{r}}$  respectively (with  $r = |\mathbf{r}|$  and  $h = |\mathbf{h}|$ ). If the spherical gravity and the  $J_2$  gravity of the Earth are considered, the motion of the chief satellite can be described by the following set of differential equations:

$$\begin{aligned}
\dot{r} &= v_x \\
\dot{v}_x &= -\mu/r^2 + h^2/r^3 - k_{J_2}/r^4(1 - 3s_i^2 s_\theta^2) \\
\dot{h} &= -(k_{J_2} s_i^2 s_{2\theta})/r^3 \\
\dot{\theta} &= h/r^2 + (2k_{J_2} c_i^2 c_\theta^2) \\
\dot{i} &= -(k_{J_2} s_{2i} s_{2\theta})/(2hr^3) \\
\dot{\Omega} &= -(2k_{J_2} c_i s_\theta^2)/(hr^3)
\end{aligned} \tag{5}$$

where, from now onwards,  $s_o = \sin(o)$ ,  $c_o = \cos(o)$ ; finally,  $k_{J_2} = 3J_2\mu R_e^2/2$  and  $R_e = 6378.137$  km is the Earth's equatorial radius.

The RSW reference frame is attached on the chief spacecraft, and its angular velocities can be expressed as function of the Eulerian angles ( $\Omega$ ,  $i$ ,  $\theta$ ):

$$\begin{aligned}
\dot{\omega}_x &= \dot{i}c_\theta + \dot{\Omega}s_\theta s_i \\
\dot{\omega}_y &= -\dot{i}s_\theta + \dot{\Omega}c_\theta s_i = 0 \\
\dot{\omega}_z &= \dot{\theta} + \dot{\Omega}c_i
\end{aligned} \tag{6}$$

The associated accelerations are

$$\begin{aligned}
\dot{\alpha}_x &= -(k_{J_2} s_{2i} c_\theta)/r^5 + (3v_x k_{J_2} s_{2i} s_\theta)/(r^4 h) - (8k_{J_2}^2 s_i^3 c_i s_\theta^2 c_\theta)/(r^6 h^2) \\
\dot{\alpha}_z &= (2v_x h)/r^3 - (k_{J_2} s_i^2 s_{2\theta})/r^5
\end{aligned} \tag{7}$$

After some manipulations [4], the exact nonlinear relative dynamics of the deputy spacecraft in the RSW frame, considering the spherical gravity and the  $J_2$  gravity of the Earth, becomes:

$$\begin{aligned}\ddot{x} &= 2\dot{y}\omega_z - x(\eta_d^2 - \omega_z^2) + y\alpha_z - z\omega_x\omega_z - (\xi_d - \xi)s_i s_\theta - r(\eta_d^2 - \eta^2) \\ \ddot{y} &= -2\dot{x}\omega_z + 2\dot{z}\omega_x - x\alpha_z - y(\eta_d^2 - \omega_z^2 - \omega_x^2) + z\alpha_x - (\xi_d - \xi)s_i c_\theta \\ \ddot{z} &= -2\dot{y}\omega_x - x\omega_x\omega_z - y\alpha_x - z(\eta_d^2 - \omega_x^2) - (\xi_d - \xi)c_i\end{aligned}\quad (8)$$

The angular velocities  $(\eta, \eta_d)$  read:

$$\begin{aligned}\eta^2 &= \mu/r^3 + k_{J_2}/r^5 - (5k_{J_2}s_i^2s_\theta^2)/r^5 \\ \eta_d^2 &= \mu/r_d^3 + k_{J_2}/r_d^5 - (5k_{J_2}r_{dZ}^2)/r_d^7\end{aligned}\quad (9)$$

and the accelerations  $(\xi, \xi_d)$  are:

$$\begin{aligned}\xi &= (2k_{J_2}s_i s_\theta)/r^4 \\ \xi_d &= (2k_{J_2}r_{dZ})/r_d^5\end{aligned}\quad (10)$$

where  $r_d$  is the geocentric distance of the deputy and  $r_{dZ}$  is the projection of  $r_d$  on the Z axis of the ECI frame.

As for the Sun-direction  $\hat{\mathbf{s}}$  in the RSW frame, it is defined by two angles:  $\psi$ , that stands for the *in-plane* direction, and  $\phi$ , that stands for the *out-of-plane* direction, with respect to the chief spacecraft reference frame (see Fig. 1). In this analysis, the direction of the Sun is governed by the following dynamics:

$$\begin{aligned}\dot{\psi} &= \dot{\omega}_z \\ \dot{\phi} &= 0\end{aligned}\quad (11)$$

#### 4. Controlled Dynamics

In this work an  $x - y - z$  spatial configuration has been considered, and *differential* solar radiation pressure has been investigated as an active way to control the system. The control accelerations, in a polar parametrization, are defined as:

$$\begin{aligned}a_x &= +\sigma\varepsilon dc_r a_{srp} c_\gamma c_\delta \\ a_y &= -\sigma\varepsilon dc_r a_{srp} s_\gamma c_\delta \\ a_z &= +\sigma\varepsilon dc_r a_{srp} s_\delta\end{aligned}\quad (12)$$

where  $\varepsilon = (\hat{\mathbf{s}} \cdot \hat{\mathbf{n}})^2$ . Moreover, as mentioned previously,  $\hat{\mathbf{s}}$  stands for the Sun-direction, while  $\hat{\mathbf{n}}$  stands for the femto-spacecraft normal component. The control acceleration is modeled as for a classic solar sail: the normalized acceleration direction due to the effect of solar radiation pressure on the sail surface, considering an ideal sail, is aligned with its normal component  $\hat{\mathbf{n}}$ . Moreover, there exists a coupling (through  $\varepsilon$ ) between the the control magnitude  $\sigma$  and the control direction given by  $\gamma$  and  $\delta$ .

A few constants appear in Eqs. 12, and they are:

- $a_{srp}$ : solar radiation acceleration, equal to  $p_{sr} \cdot r_{am}$ ;
- $p_{sr}$ : solar radiation pressure, equal to  $W/c_{light} = 4.56 \times 10^{-6} \text{ N/m}^2$  (with  $W$  the energy flux density of the Sun at 1 AU and  $c_{light}$  the speed of light);
- $r_{am}$ : area-to-mass ratio, equal to  $10^1 \text{ m}^2\text{kg}^{-1}$ ;
- $dc_r$ : differential reflectivity coefficient;
- $\gamma$ : azimuth control direction;
- $\delta$ : elevation control direction;
- $\sigma$ : control magnitude  $\in [0, 1]$  (full control capability femto-spacecraft) or  $\in [-1, 1]$  (limited control capability femto-spacecraft).

The nominal formation-flying shape investigated is a GCO (according to the linearized CWH dynamics of Eqs. 1, neglecting perturbation [7]), where the relative motion is a circle in the three-dimensional space  $x - y - z$ .

Thanks to the high area-to-mass ratio of the micro-spacecraft taken in consideration, solar radiation pressure reveals to be useful to control the relative motion within the formation in reasonable time. It is assumed that it is possible to change the value of the differential reflectivity coefficient  $dc_r$  by means of electrochromic control. Considering that the Sun-facing side of the micro-spacecraft is either completely absorptive ( $c_r = 1$ ) or completely reflective ( $c_r = 2$ ), in this work the chief is assumed to have a reflectivity coefficient  $c_r = 1.5$ , while the deputy can change its value from  $c_r = 1.25$  to  $c_r = 1.75$  [3]. The differential reflectivity coefficient  $dc_r$  introduced in Eqs. 12 is assumed equal to the maximum value  $+0.25$ .

## 5. Optimal Control Problem

This paper deals with the application of the theory of optimal control, based on its fundamental background in the associated calculus of variations. A brief explanation is presented in the following: a simple problem with no path but only equality constraints is considered [8].

Assuming a differential system of  $n$  first-order equations describing a generic dynamics, that is:

$$\dot{\mathbf{y}} = \mathbf{f}[\mathbf{y}(t), \mathbf{u}(t), t], \quad (13)$$

where  $\mathbf{y}(t_i)$  is given and  $t_i \leq t \leq t_f$ . The control function  $\mathbf{u}(t)$  is chosen to minimize the following performance index:

$$J = \varphi[\mathbf{y}(t_f), t_f] + \int_{t_i}^{t_f} L[\mathbf{y}(t), \mathbf{u}(t), t] dt, \quad (14)$$

subject to  $q$ -dimensional final boundary conditions:

$$\chi_f[\mathbf{y}(t_f), \mathbf{u}(t_f), t_f] = 0. \quad (15)$$

It is possible to notice that there are continuous equality constraints (Eqs. 13) as well as discrete ones (Eqs. 15).

Introducing the  $q$ -dimensional vector of Lagrange multipliers  $\mathbf{v}(t)$  associated with the final boundary constraints, and the  $n$ -dimensional vector of adjoint or costate variables  $\lambda(t)$  for the dynamics,

the augmented performance is defined as:

$$\begin{aligned} \hat{J} = & \varphi [\mathbf{y}(t_f), t_f] + \mathbf{v}^\top \boldsymbol{\chi} [\mathbf{y}(t_f), \mathbf{u}(t_f), t_f] + \\ & + \int_{t_i}^{t_f} L[\mathbf{y}(t), \mathbf{u}(t), t] + \boldsymbol{\lambda}^\top \{\mathbf{f}[\mathbf{y}(t), \mathbf{u}(t), t] - \dot{\mathbf{y}}\} dt. \end{aligned} \quad (16)$$

The conditions required for optimality are obtained setting the first derivatives of  $\hat{J}$  to zero, namely  $\delta \hat{J} = 0$ , which correspond to the search of its stationary point. In order to present the formulation in a compact form, it is convenient to define the Hamiltonian of the problem, that is the scalar function:

$$H[\mathbf{y}(t), \mathbf{u}(t), \boldsymbol{\lambda}(t), t] = L[\mathbf{y}(t), \mathbf{u}(t), t] + \boldsymbol{\lambda}^\top \mathbf{f}[\mathbf{y}(t), \mathbf{u}(t), t] \quad (17)$$

and the auxiliary function:

$$\vartheta = \varphi + \mathbf{v}^\top \boldsymbol{\chi}. \quad (18)$$

The necessary conditions referred to as *Euler-Lagrange equations* in the calculus of variation, that result from forcing the first variation to zero, and integrating by parts the last term on the right side of Eq. 17, in addition to Eqs. 14 and Eqs. 15 are:

$$\dot{\boldsymbol{\lambda}} = - \left[ \frac{\partial H}{\partial \mathbf{y}} \right]^\top, \quad (19)$$

called adjoint equations describing the dynamics of the co-states,

$$0 = \left[ \frac{\partial H}{\partial \mathbf{u}} \right]^\top, \quad (20)$$

known as algebraic equations for the control functions, and

$$\boldsymbol{\lambda}(t_f) = \boldsymbol{\vartheta}|_{t_f}, \quad 0 = (\boldsymbol{\vartheta}_t + H)|_{t_f}, \quad 0 = \boldsymbol{\lambda}(t_i), \quad (21)$$

called transversality conditions. The problem, as stated previously, is known as *two-point boundary-value problem*, TPBVP [8].

The control Eqs. 20 are an application of the Pontryagin maximum principle. A more general expression is:

$$\mathbf{u}(t) = \arg \min_{\mathbf{u} \in U} H[\mathbf{y}(t), \mathbf{u}(t), \boldsymbol{\lambda}(t), t], \quad (22)$$

where  $U$  defines the domain of feasible controls. The maximum principle states that the control variables are chosen to optimize the Hamiltonian at every instant of time. In essence Eq. 22 is a constrained optimization problem in the variables  $\mathbf{u}(t)$ , for all values of  $t$ . The complete set of necessary conditions consists of a differential-algebraic (DAE) system.

The problem is also subjected to initial conditions:

$$\mathbf{y}(t_i) = \mathbf{y}_i, \quad (23)$$

and to final conditions:

$$\mathbf{y}(t_f) = \mathbf{y}_f. \quad (24)$$

## 5.1. Fixed Final Time Problem

The first-order complete controlled dynamic system is:

$$\begin{aligned}
\dot{r} &= v_x \\
\dot{v}_x &= -\mu/r^2 + h^2/r^3 - k_{J_2}/r^4(1 - 3s_i^2s_\theta^2) \\
\dot{h} &= -(k_{J_2}s_i^2s_{2\theta})/r^3 \\
\dot{\theta} &= h/r^2 + (2k_{J_2}c_i^2c_\theta^2) \\
\dot{i} &= -(k_{J_2}s_{2i}s_{2\theta})/(2hr^3) \\
\dot{\Omega} &= -(2k_{J_2}c_i s_\theta^2)/(hr^3) \\
\dot{x} &= v_x \\
\dot{y} &= v_y \\
\dot{z} &= v_z \\
\dot{v}_z &= 2v_y\omega_z - x(\eta_d^2 - \omega_z^2) + y\gamma_z - z\omega_x\omega_z - (\xi_d - \xi)s_i s_\theta - r(\eta_d^2 - \eta^2) + \sigma\epsilon dc_r a_{srp} c_\gamma c_\delta \\
\dot{v}_y &= -2v_x\omega_z + 2v_z\omega_x - x\alpha_z - y(\eta_d^2 - \omega_z^2 - \omega_x^2) + z\alpha_x - (\xi_d - \xi)s_i c_\theta - \sigma\epsilon dc_r a_{srp} s_\gamma c_\delta \\
\dot{v}_x &= -2v_y\omega_x - x\omega_x\omega_z - y\alpha_x - z(\eta_d^2 - \omega_x^2) - (\xi_d - \xi)c_i + \sigma\epsilon dc_r a_{srp} s_\delta
\end{aligned} \tag{25}$$

In a fixed time scenario, assuming that  $J$  doesn't depend on the final states and final time and that is only a function of the controls (and not the states), i.e.:

$$J = \int_{t_i}^{t_f} L[\mathbf{u}(t)] dt, \tag{26}$$

the Hamiltonian reads:

$$\begin{aligned}
H &= L + \lambda_r(v_x) + \lambda_{v_x}(-\mu/r^2 + h^2/r^3 - k_{J_2}/r^4(1 - 3s_i^2s_\theta^2)) + \lambda_h(-(k_{J_2}s_i^2s_{2\theta})/r^3) + \\
&+ \lambda_\theta(h/r^2 + (2k_{J_2}c_i^2c_\theta^2)) + \lambda_i(-(k_{J_2}s_{2i}s_{2\theta})/(2hr^3)) + \lambda_\Omega(-(2k_{J_2}c_i s_\theta^2)/(hr^3)) + \\
&+ \lambda_x v_x + \lambda_y v_y + \lambda_z v_z + \\
&+ \lambda_{v_x}(+2v_y\omega_z - x(\eta_d^2 - \omega_z^2) + y\alpha_z - z\omega_x\omega_z - (\xi_d - \xi)s_i s_\theta - r(\eta_d^2 - \eta^2) + \sigma\epsilon dc_r a_{srp} c_\gamma c_\delta) + \\
&+ \lambda_{v_y}(-2v_x\omega_z + 2v_z\omega_x - x\alpha_z - y(\eta_d^2 - \omega_z^2 - \omega_x^2) + z\alpha_x - (\xi_d - \xi)s_i c_\theta - \sigma\epsilon dc_r a_{srp} s_\gamma c_\delta) + \\
&+ \lambda_{v_z}(-2v_y\omega_x - x\omega_x\omega_z - y\alpha_x - z(\eta_d^2 - \omega_x^2) - (\xi_d - \xi)c_i + \sigma\epsilon dc_r a_{srp} s_\delta)
\end{aligned} \tag{27}$$

and the dynamics of the co-states follows directly from Eqs. 19.

## 5.2. Free Final Time Problem

In a free time scenario, the following transversality condition is added to the overall system:

$$(\vartheta_t + H)|_{t_f} = 0. \tag{28}$$

Eqs. 25 and Eqs. 19 constitute a set of 24 ordinary differential equations, whose boundary conditions are given by the initial conditions (Eqs. 23) and the final conditions (Eqs. 24). This two-point boundary value problem is highly non-linear and thus should be numerically solved. To that end, a Matlab routine, called *bvp4c*, which is based on collocation methods, is utilized.

Unfortunately, the standard form doesn't match this type of problem, because the time period is defined to be fixed:  $t \in [a, b]$ .

Key step is to re-scale time so that  $\tau = t/t_f$ , then  $t \in [0, 1]$ . Implications of this scaling are that the derivatives must be changed since  $d\tau = dt/t_f$ :

$$\frac{d}{d\tau} = t_f \frac{d}{dt}. \quad (29)$$

Final step is to introduce a dummy state  $r$  that corresponds to  $t_f$  with the trivial dynamics  $\dot{r} = 0$ . Replacing all instances of  $t_f$  in the necessary/boundary conditions for state  $r$ . The optimizer will then just pick an appropriate constant for  $r = t_f$ .

## 6. Test Cases

Two different applicative scenarios have been investigated in this paper: firstly, a combined reconfiguration maneuver with the aim of changing the amplitude and of shifting the centre of a GCO is investigated (according to the linearized CWH dynamics of Eqs. 1, neglecting perturbation). Secondly, a maneuver to maintain the nominal formation configuration is presented. Both of these maneuvers have been solved assuming three different performance indexes:  $L = \sigma$ ,  $L = \frac{1}{2}\sigma^2$  and the minimum time problem.

Moreover, two different control authorities have been considered in this work:

- full control capability: the *deputy* femto-spacecraft is able to align its normal  $\hat{\mathbf{n}}$  in the direction given by the solution of the optimal control problem; as for a classic solar sail scenario, the acceleration magnitude is directed along  $\hat{\mathbf{n}}$  and is scaled by  $\varepsilon$ .
- limited control capability: the *deputy* femto-spacecraft is designed to be passively Sun-pointing [9]; again, as for a classic solar sail scenario, the acceleration magnitude is directed along  $\hat{\mathbf{n}}$ ; in this particular case,  $\hat{\mathbf{n}} \equiv \hat{\mathbf{s}}$ , leading to  $\varepsilon = 1$ .

As far as it concerns the orbital elements for the chief micro-spacecraft, their initial values are listed below [10]:

- $a$ : semimajor axis, equal to 7153.137 km;
- $e$ : eccentricity, equal to 0.05;
- $i$ : inclination, equal to 48.0 deg;
- $\Omega$ : longitude of the ascending node, equal to 45.0 deg;
- $\omega$ : anomaly of the pericentre, equal to 0.0 deg;
- $M$ : mean anomaly, equal to 90.0 deg.

As for the reconfiguration maneuver scenario, starting from amplitudes  $a_i = 100$  m and  $b_i = \sqrt{3}/2$ .

100 m, the deputy micro-spacecraft is driven to a larger relative orbit, with amplitudes  $a_f = 110$  m and  $b_f = \sqrt{3}/2 \cdot 110$  m. The initial and final angular positions of the deputy along the periodic relative orbit are assumed as  $\alpha_i = \alpha_f = \pi/2$  and as  $\beta_i = \beta_f = -\pi/2$ . Initially the Sun-direction, in the  $x - y$  plane, is aligned with the opposite direction of the transverse axis, i.e. along the  $-y$  axis with  $\psi_i = \pi/2$ , while the out-of-plane Sun-direction angle is  $\phi = 0.5 \cdot \pi/2$ . Moreover, starting from an initial location of the centre along the  $y$  axis, i.e.,  $c_i = 0$  m, the deputy micro-spacecraft is driven to a relative orbit, with a centre location shifted to  $c_f = +10$  m. The maneuver time is set equal to 1 orbital periods.

As far as it concerns the maintenance maneuver scenario, the initial and final amplitudes are  $a_i = 110$  m,  $b_i = \sqrt{3}/2 \cdot 110$  m,  $a_f = 110$  m and  $b_f = \sqrt{3}/2 \cdot 110$  m. The initial and final angular positions of the deputy along the periodic relative orbit are assumed as  $\alpha_i = \alpha_f = \pi/2$  and as  $\beta_i = \beta_f = -\pi/2$ . Initially the Sun-direction, in the  $x - y$  plane, is aligned with the opposite direction of the transverse axis, i.e. along the  $-y$  axis with  $\psi_i = \pi/2$ , while the out-of-plane Sun-direction angle is  $\phi = 0.5 \cdot \pi/2$ . Moreover, the location of centre along the  $y$  axis is kept at  $c_i = 0$  m and  $c_f = 0$  m. The maneuver time is set equal to 1 orbital periods.

The total Hamiltonian  $H$  is minimized as a function of  $(\sigma, \gamma, \delta)$ . As far as it concerns  $\varepsilon$ , a linear combination is implemented:

$$\varepsilon = (1 - q_\varepsilon) \cdot \varepsilon_a + (q_\varepsilon) \cdot \varepsilon_b, \quad rcl \quad (30)$$

where  $q_\varepsilon \in [0, 1]$  is the parameter introduced to perform a continuation process,  $\varepsilon_a = 1$  and  $\varepsilon_b = (\hat{\mathbf{s}} \cdot \hat{\mathbf{n}})^2$ .

For the full control capability femto-spacecraft, the continuation approach starts with  $q_\varepsilon = 0$  and then the obtained solution is used as the next initial guess for the next run, where  $q_\varepsilon$  is increased till it reaches 1. On the other hand, in case of the limited control capability femto-spacecraft, there is no need of this continuation process, and a coherent solution is found already with  $q_\varepsilon = 0$ .

Therefore, as far as it concerns the angular components of the control vector for the full control capability femto-spacecraft, the global minimum of the Hamiltonian  $H$  is found either at

$$\begin{cases} \gamma^{1*} = \arctan - \left( \frac{\lambda_{v_y}}{\lambda_{v_x}} \right) \\ \delta^{1*} = \arctan \left( \frac{\lambda_{v_z}}{\lambda_{v_x} c \gamma^* - \lambda_{v_y} s \gamma^*} \right) \end{cases} \quad (31)$$

or at

$$\begin{cases} \gamma^{2*} = \gamma^{1*} + \pi \\ \delta^{2*} = \delta^{1*} \end{cases} \quad (32)$$

$H$  is computed at both two solution candidates given by Eq. 31 and Eq. 32; the candidate that yields the lowest  $H$  allows to choose the optimal set of  $\gamma^*$  and  $\delta^*$ . If  $\lambda_{v_x} = \lambda_{v_y} = 0$  for some  $t$ ,  $\gamma$

is irrelevant and  $\delta = -\text{sign}(\lambda_{v_z})\pi/2$ . In this case,  $\sigma$  is bounded between  $[0, 1]$ , and the optimal control angles describe the control direction.

As for the limited control capability femto-spacecraft case, two more continuation processes are introduced in order to augment the optimal control problem with path constraints on the control angles:

$$\begin{aligned}\gamma &= (1 - q_\gamma) \cdot \gamma_a + (q_\gamma) \cdot \gamma_b \\ \delta &= (1 - q_\delta) \cdot \delta_a + (q_\delta) \cdot \delta_b\end{aligned}\tag{33}$$

Both  $q_\gamma \in [0, 1]$  and  $q_\delta \in [0, 1]$  are the continuation parameters, while  $\gamma_a$  and  $\delta_a$  stand for  $\gamma^*$  and  $\delta^*$ , respectively. On the other hand,  $\gamma_b$  and  $\delta_b$  correspond to the Sun-direction, i.e.  $\gamma_b = \psi$  and  $\delta_b = \phi$  for each time step. Again, the continuation approaches start with  $q_\gamma = 0$  and  $q_\delta = 0$ ; then the obtained solution is used as the next initial guess for the next run, where  $q_\gamma$  and  $q_\delta$  are increased till they reach 1. In this case,  $\sigma$  is bounded between  $[-1, 1]$ : a positive value means the relative control acceleration is aligned with the Sun-direction, a negative one means it is in the opposite direction.

### 6.1. Case 1: Minimum $\sigma$ Problem

As far as it concerns the first test case, the objective function taken into consideration is:

$$J = \int_{t_i}^{t_f} \sigma \, dt.\tag{34}$$

As stated previously, the aim is to minimize the global Hamiltonian as a function of  $(\sigma, \gamma, \delta)$ . Notice that, for the full control capability femto-spacecraft, even though  $\sigma$  can only be 0 or 1 in this case, for the optimal control problem statement, it is assumed to belong to  $\sigma \in [0, 1]$ . The optimal solution will set it as 0 or 1. On the other hand, for the limited control capability femto-spacecraft, even though  $\sigma$  can only be  $-1$  or  $1$  in this case, for the optimal control problem statement, it is assumed to belong to  $\sigma \in [-1, 1]$ . The optimal solution will set it as  $-1$  or  $1$ .

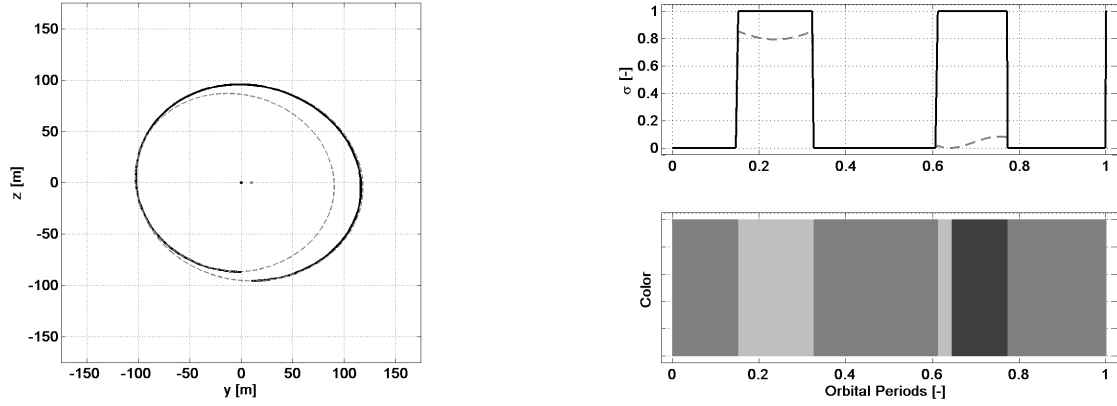
Define the switching function  $S_\sigma$  as

$$\begin{aligned}S_\sigma &= 1 + \lambda_{v_x} dc_r a_{srp} c_\gamma c_\delta + \\ &\quad - \lambda_{v_y} dc_r a_{srp} s_\gamma c_\delta + \\ &\quad + \lambda_{v_z} dc_r a_{srp} s_\delta\end{aligned}\tag{35}$$

Then,

$$\sigma = \begin{cases} 1, & \text{if } S_\sigma < 0, \\ 0, & \text{if } S_\sigma \geq 0 \end{cases}\tag{36}$$

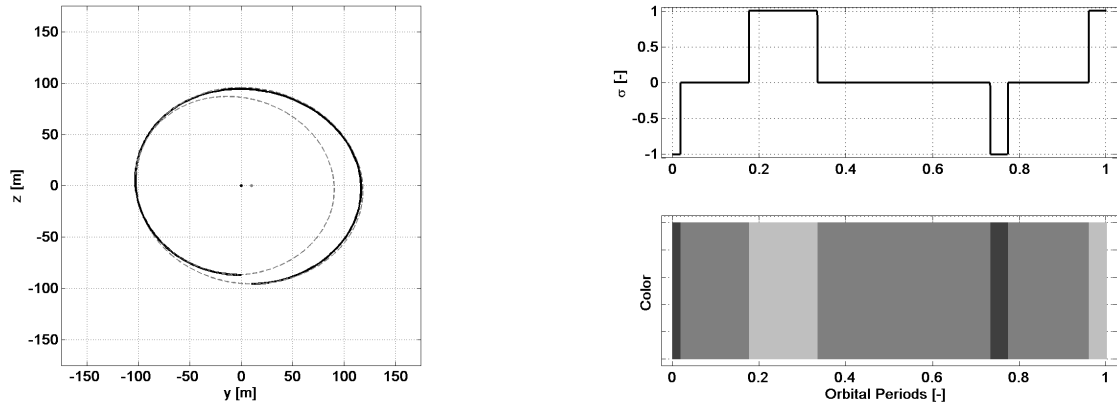
This two-point boundary value problem is solved numerically via the aforementioned Matlab routine *bvp4c*, which is based on collocation methods. However, due to the discontinuous behavior of



(a) Reconfiguration maneuver,  $y - z$  plane view.

(b) Control magnitude  $\sigma$ . The dashed line is  $\sigma \cdot \epsilon$ .

Figure 3. Reconfiguration maneuver (Case 1) for full control capability femto-spacecraft: relative motion and control magnitude.



(a) Reconfiguration maneuver,  $y - z$  plane view.

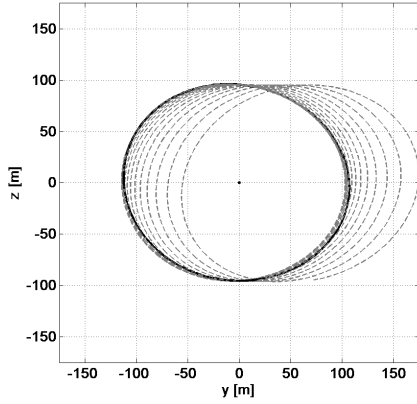
(b) Control magnitude  $\sigma$ .

Figure 4. Reconfiguration maneuver (Case 1) for limited control capability femto-spacecraft: relative motion and control magnitude.

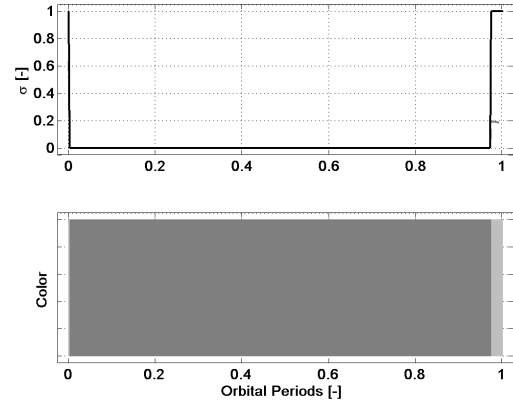
$\sigma$ , it is not possible to obtain a solution from the numerical solver, as it was designed for continuous dynamical systems. In order to implement the binary control law for  $\sigma$  as smooth function, amenable for the numerical processing, Eq. 36 is replaced by

$$\sigma = -\frac{\arctan(q_\sigma S_\sigma) + \pi/2}{\pi} + 1 \quad (37)$$

where  $q_\sigma$  is a parameter utilized to perform a continuation process to numerically solve the two-point boundary value problem. As  $q_\sigma$  tends to infinity, Eq. 37 tends to the corresponding binary function. The numerical solver *bvp4c* relies on initial guesses for the whole solution. Hence, to obtain a good initial guess, it is necessary to start with low values (order of magnitude of 1) of  $q_\sigma$ , and then the obtained solution is used as the next initial guess for the next run, where  $q_\sigma$  is increased by an order of magnitude. The process is iteratively continued until a high enough value of  $q_\sigma$  is reached, such that the obtained thrust profile is bang-off-bang. At orders of magnitude of

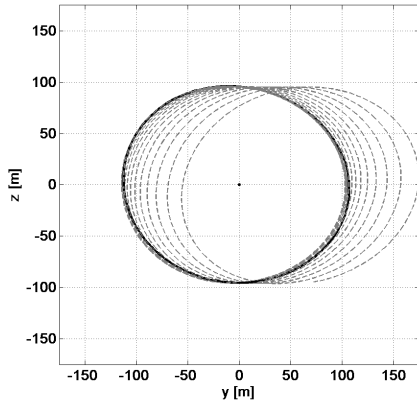


(a) Maintenance maneuver,  $y-z$  plane view.

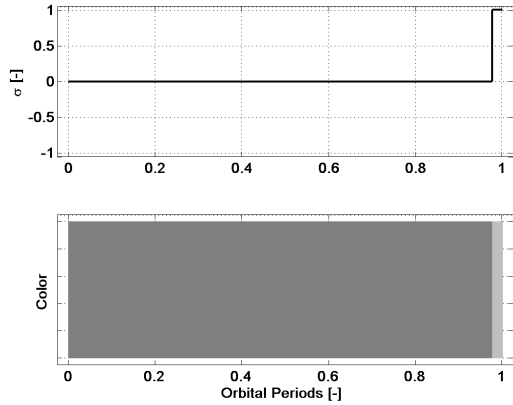


(b) Control magnitude  $\sigma$ . The dashed line is  $\sigma \cdot \varepsilon$ .

Figure 5. Maintenance maneuver (Case 1) for full control capability femto-spacecraft: relative motion and control magnitude.



(a) Maintenance maneuver,  $y-z$  plane view.

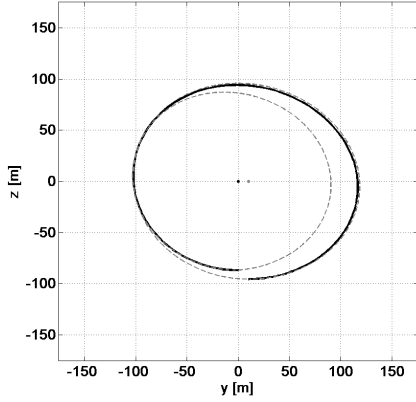


(b) Control magnitude  $\sigma$ .

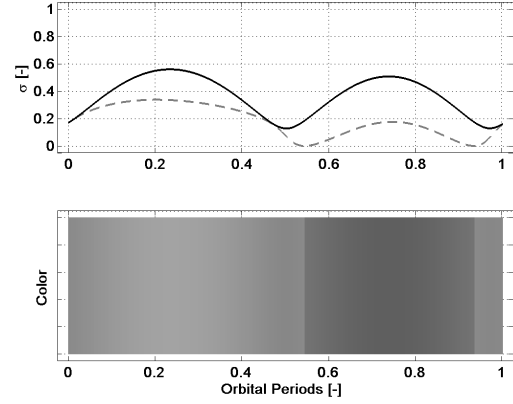
Figure 6. Maintenance maneuver (Case 1) for limited control capability femto-spacecraft: relative motion and control magnitude.

$10^4$ , the thrust profile is already perceived as bang-off-bang (see Fig. 3(b), Fig. 4(b), Fig. 5(b) and Fig. 6(b)).

As for the reconfiguration maneuver scenario, the problem has been solved both with fixed final (equal to 1 nominal orbital period, i.e.  $t_f = 6020.7$  s) time and with free final time, that the optimization process selects as  $t_f = 6027.1$  s (full control capability femto-spacecraft) and as  $t_f = 6028.3$  s (limited control capability femto-spacecraft). Besides the maneuver time, all the other reconfiguration parameters are very similar for the two scenarios investigated. For the maintenance maneuver scenario, as in the previous case, the problem has been solved both with fixed final (equal to 1 nominal orbital period, i.e.  $t_f = 6020.7$  s) time and with free final time, that the optimization process selects as  $t_f = 6024.3$  s (full control capability femto-spacecraft) and as  $t_f = 6025.1$  s (limited control capability femto-spacecraft). Besides the maneuver time, all the

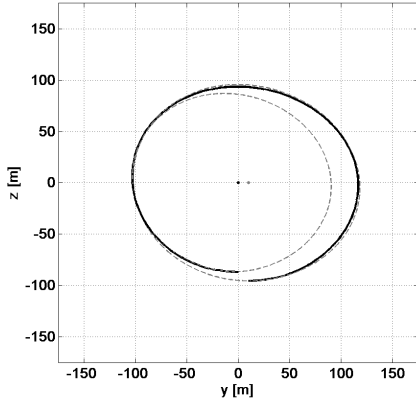


(a) Reconfiguration maneuver,  $y - z$  plane view.

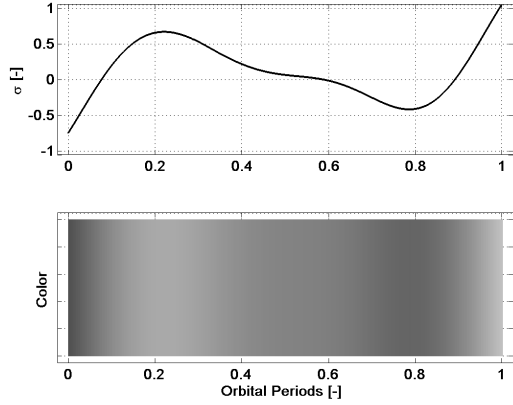


(b) Control magnitude  $\sigma$ . The dashed line is  $\sigma \cdot \epsilon$ .

Figure 7. Reconfiguration maneuver (Case 2) for full control capability femto-spacecraft: relative motion and control magnitude.



(a) Reconfiguration maneuver,  $y - z$  plane view.



(b) Control magnitude  $\sigma$ .

Figure 8. Reconfiguration maneuver (Case 2) for limited control capability femto-spacecraft: relative motion and control magnitude.

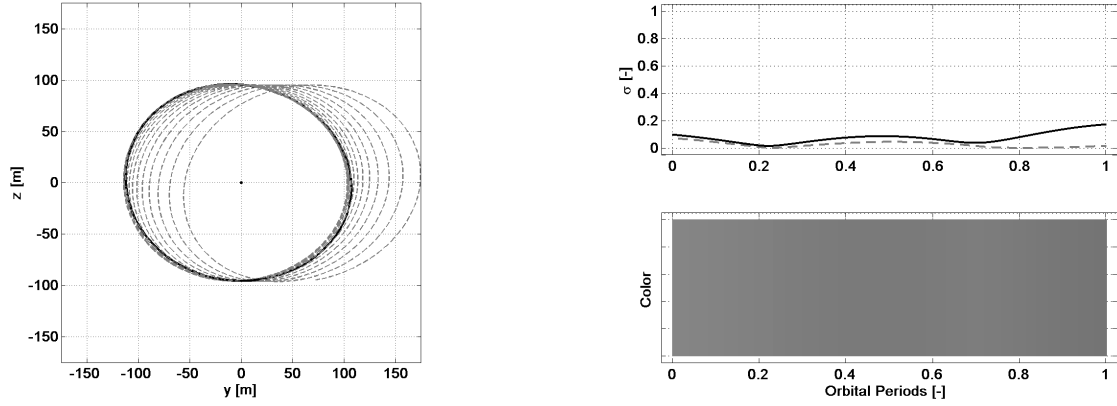
other reconfiguration parameters are very similar for the two scenarios investigated. The dashed lines in Fig. 5(a) and Fig. 6(a) stand for the evolution, under the nonlinear dynamics, of the relative motion, propagated for 1 day without the maintenance maneuver.

## 6.2. Case 2: Minimum $\frac{1}{2}\sigma^2$ Problem

The objective function investigated in this test case is:

$$J = \int_{t_i}^{t_f} \frac{1}{2} \sigma^2 dt. \quad (38)$$

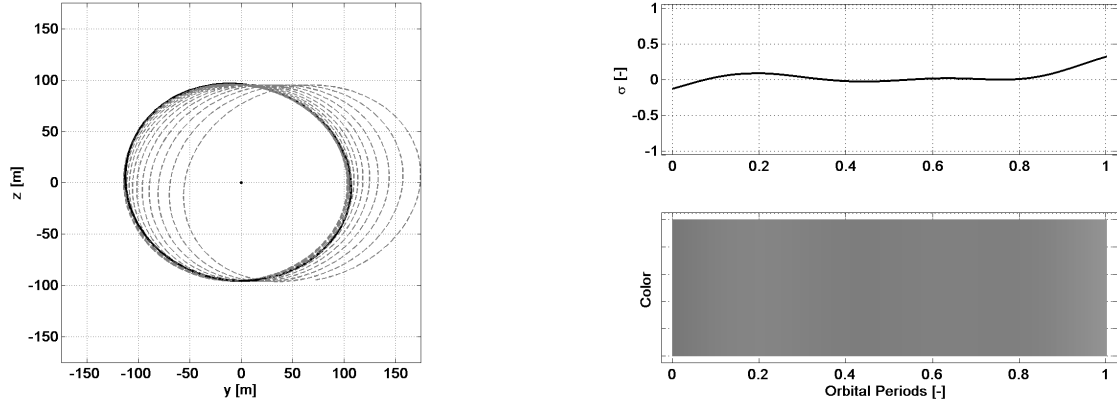
Aiming at minimizing the global Hamiltonian as a function of  $(\sigma, \gamma, \delta)$ , the global minimum of  $H$



(a) Maintenance maneuver,  $y - z$  plane view.

(b) Control magnitude  $\sigma$ . The dashed line is  $\sigma \cdot \epsilon$ .

Figure 9. Maintenance maneuver (Case 2) for full control capability femto-spacecraft: relative motion and control magnitude.



(a) Maintenance maneuver,  $y - z$  plane view.

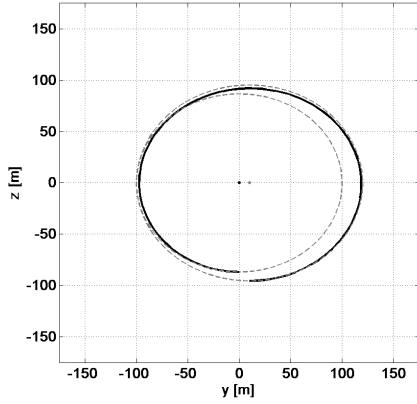
(b) Control magnitude  $\sigma$ .

Figure 10. Maintenance maneuver (Case 2) for limited control capability femto-spacecraft: relative motion and control magnitude.

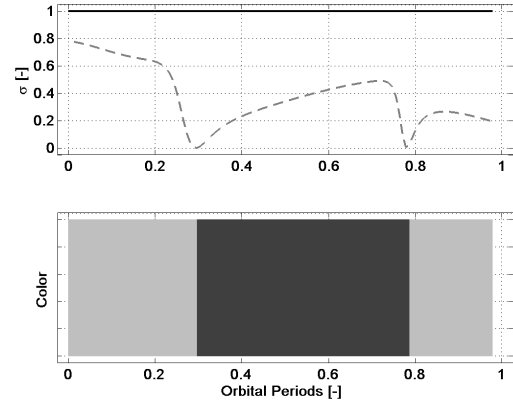
is found at (see Fig. 7)

$$\begin{aligned}
 \sigma = & -\lambda_{v_x} dc_r a_{srp} c \gamma c_\delta + \\
 & + \lambda_{v_y} dc_r a_{srp} s \gamma c_\delta + \\
 & - \lambda_{v_z} dc_r a_{srp} s \delta
 \end{aligned} \tag{39}$$

As far as it concerns the reconfiguration maneuver scenario, Fig. 7 and Fig. 8 offer a view the maneuver: in 1 orbital periods the prescribed final conditions are achieved. This problem has been solved both with fixed final (equal to 1 nominal orbital period, i.e.  $t_f = 6020.7$ s) time and with free final time, that the optimization process selects as  $t_f = 6026.7$ s (full control capability femto-spacecraft) and as  $t_f = 6026.1$ s (limited control capability femto-spacecraft). Besides the maneuver time, all the other reconfiguration parameters are very similar for the two scenarios

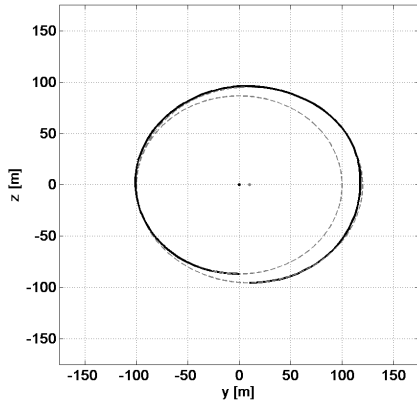


(a) Reconfiguration maneuver,  $y - z$  plane view.

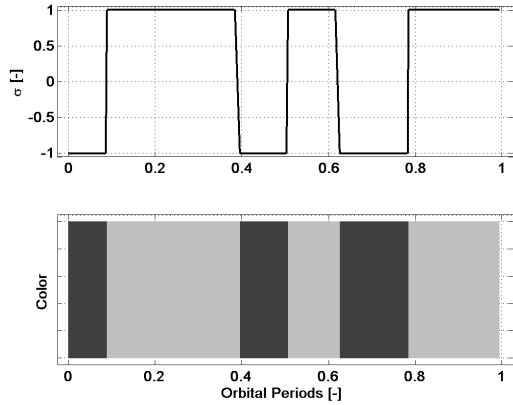


(b) Control magnitude  $\sigma$ . The dashed line is  $\sigma \cdot \epsilon$ .

Figure 11. Reconfiguration maneuver (Case 3) for full control capability femto-spacecraft: relative motion and control magnitude.



(a) Reconfiguration maneuver,  $y - z$  plane view.

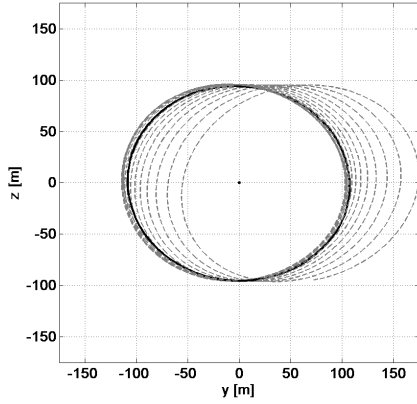


(b) Control magnitude  $\sigma$ .

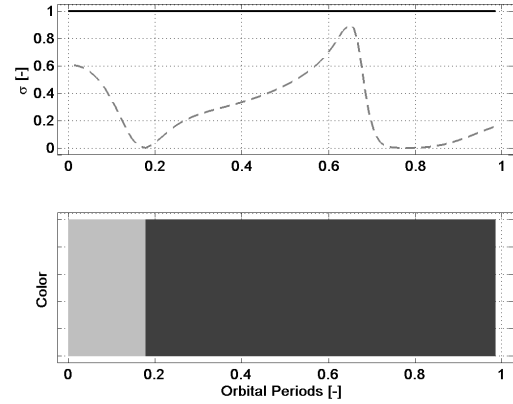
Figure 12. Reconfiguration maneuver (Case 3) for limited control capability femto-spacecraft: relative motion and control magnitude.

investigated.

For the maintenance maneuver scenario, Fig. 9 and Fig. 10 offer a view the maneuver: in 1 orbital periods the prescribed final conditions are achieved. Again, this problem has been solved both with fixed final (equal to 1 nominal orbital period, i.e.  $t_f = 6020.7$  s) time and with free final time, that the optimization process selects as  $t_f = 6024.2$  s (full control capability femto-spacecraft) and as  $t_f = 6027.4$  s (limited control capability femto-spacecraft). Besides the maneuver time, all the other reconfiguration parameters are very similar for the two scenarios investigated. The dashed lines in Fig. 9(a) and Fig. 10(a) stand for the evolution, under the nonlinear dynamics, of the relative motion, propagated for 1 day without the maintenance maneuver.

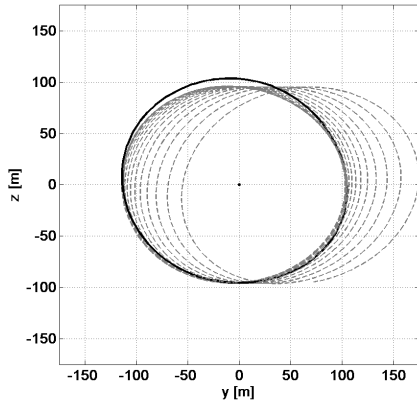


(a) Maintenance maneuver,  $y - z$  plane view.

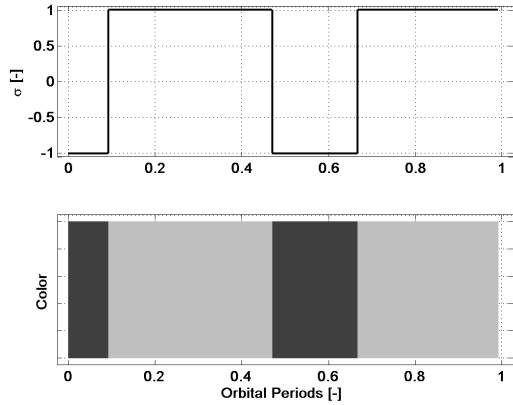


(b) Control magnitude  $\sigma$ . The dashed line is  $\sigma \cdot \epsilon$ .

Figure 13. Maintenance maneuver (Case 3) for full control capability femto-spacecraft: relative motion and control magnitude.



(a) Maintenance maneuver,  $y - z$  plane view.



(b) Control magnitude  $\sigma$ .

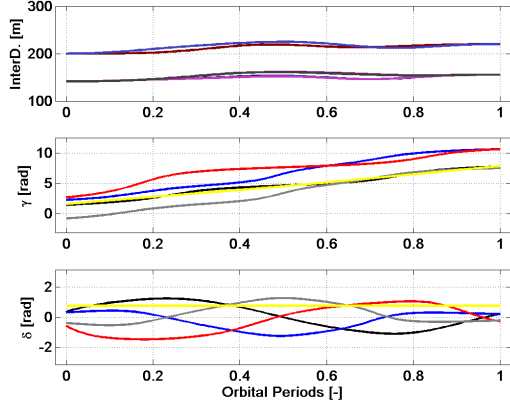
Figure 14. Maintenance maneuver (Case 3) for limited control capability femto-spacecraft: relative motion and control magnitude.

### 6.3. Case 3: Minimum Time Problem

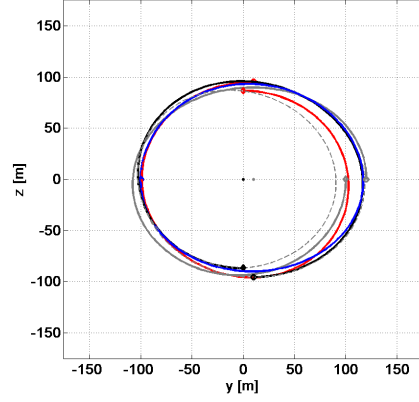
As final case, the minimum time problem is analyzed. Therefore, the performance index investigated becomes:

$$J = \int_{t_i}^{t_f} 1 dt. \quad (40)$$

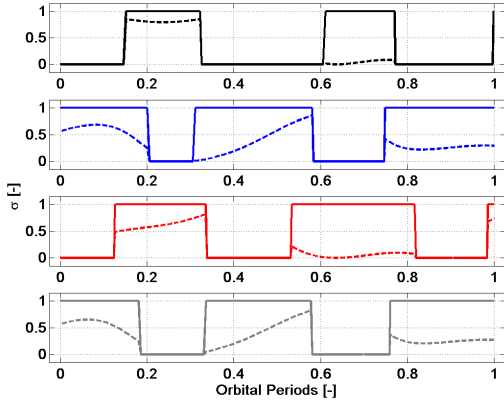
Once again, the aim is to find the global minimum of the Hamiltonian. A new switching function



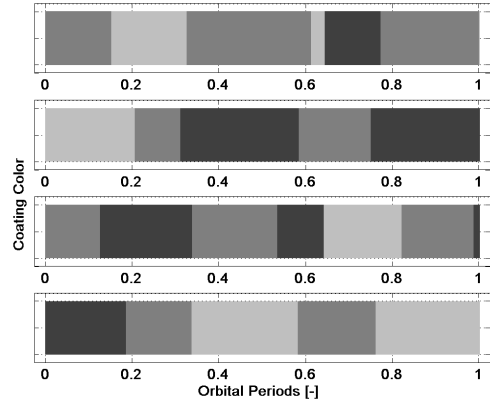
(a) Femto-spacecraft inter-distance and control directions.



(b) Reconfiguration maneuver,  $y-z$  plane view.



(c) Control magnitude  $\sigma$ . The dashed line is  $\sigma \cdot \varepsilon$ .



(d) Differential coating color.

Figure 15. Reconfiguration maneuver (Case 1) for full control capability multiple femto-spacecraft scenario: relative motion and control magnitude.

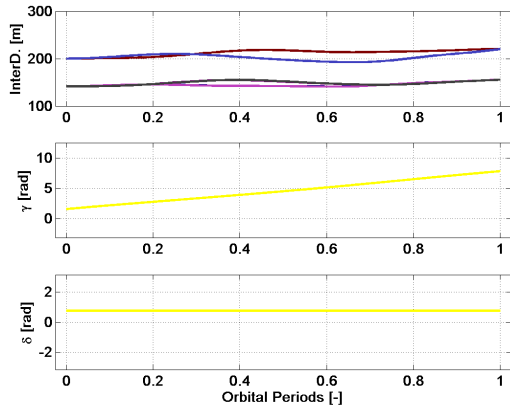
$S_\sigma$  is defined as

$$\begin{aligned}
 S_\sigma = & 0 + \lambda_{v_x} dc_r a_{srp} c_\gamma c_\delta + \\
 & - \lambda_{v_y} dc_r a_{srp} s_\gamma c_\delta + \\
 & + \lambda_{v_z} dc_r a_{srp} s_\delta
 \end{aligned} \tag{41}$$

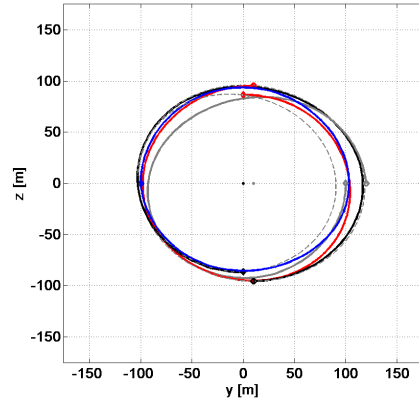
Then,

$$\sigma = \begin{cases} 1, & \text{if } S_\sigma < 0, \\ 0, & \text{if } S_\sigma \geq 0 \end{cases} \tag{42}$$

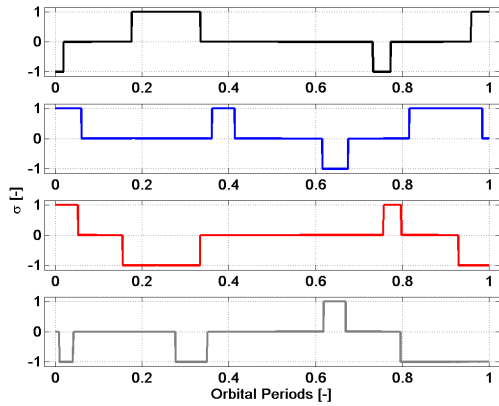
As the problem is solved numerically, the same observations written previously also hold here (see Fig. 11, Fig. 12, Fig. 13 and Fig. 14). In the reconfiguration maneuver scenario, the optimization process minimizes the final maneuver time, selecting  $t_f = 5882.3\text{s}$  (full control capability femto-spacecraft) and as  $t_f = 5974.8\text{s}$  (limited control capability femto-spacecraft), while for the



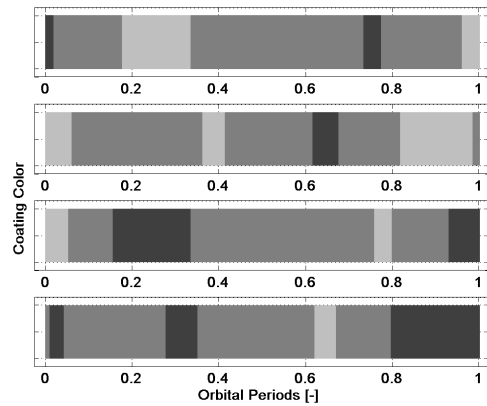
(a) Femto-spacecraft inter-distance and control directions.



(b) Reconfiguration maneuver,  $y-z$  plane view.



(c) Control magnitude  $\sigma$ .



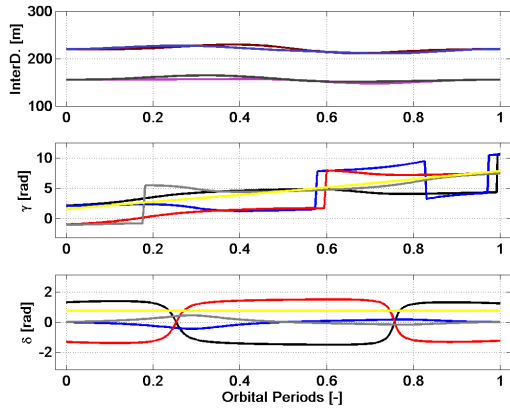
(d) Differential coating color.

Figure 16. Reconfiguration maneuver (Case 1) for limited control capability multiple femto-spacecraft scenario: relative motion and control magnitude.

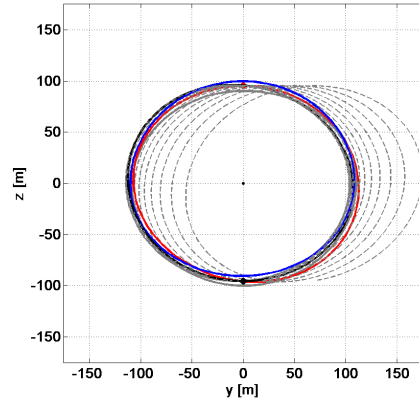
maintenance maneuver  $t_f = 5919.8$  s (full control capability femto-spacecraft) and as  $t_f = 5979.7$  s (limited control capability femto-spacecraft). With respect to the previous test cases, the control is always on duty, for both the reconfiguration and maintenance scenarios (see Fig. 11(b), Fig. 12(b), Fig. 13(b) and Fig. 14(b)). The dashed lines in Fig. 13(a) and Fig. 14(a) stand for the evolution, under the nonlinear dynamics, of the relative motion, propagated for 1 day without the maintenance maneuver.

## 6.4. Multiple Spacecraft

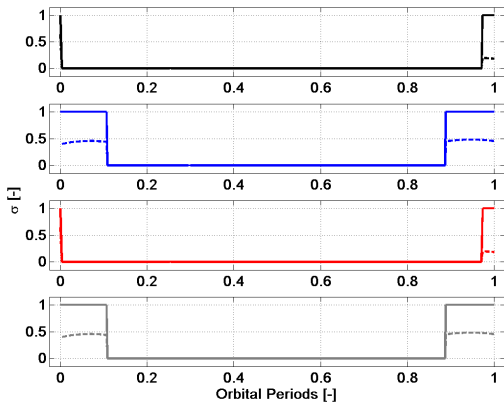
In this section a multiple spacecraft scenario is investigated. Assuming the reconfiguration and maintenance maneuvers introduced above, formations with 4 deputy spacecraft (uniformly spaced) have been considered. As for the optimal control problem, the objective function taken into con-



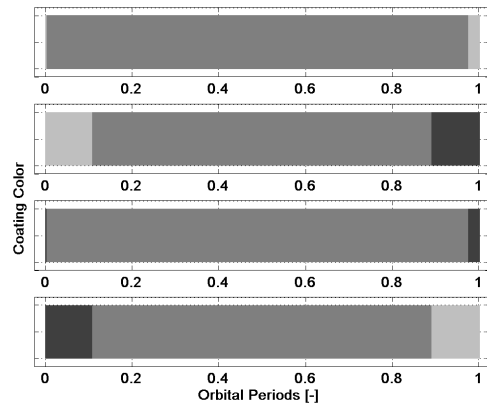
(a) Femto-spacecraft inter-distance and control directions.



(b) Reconfiguration maneuver,  $y - z$  plane view.



(c) Control magnitude  $\sigma$ . The dashed line is  $\sigma \cdot \varepsilon$ .



(d) Differential coating color.

Figure 17. Reconfiguration maneuver (Case 1) for full control capability multiple femto-spacecraft scenario: relative motion and control magnitude.

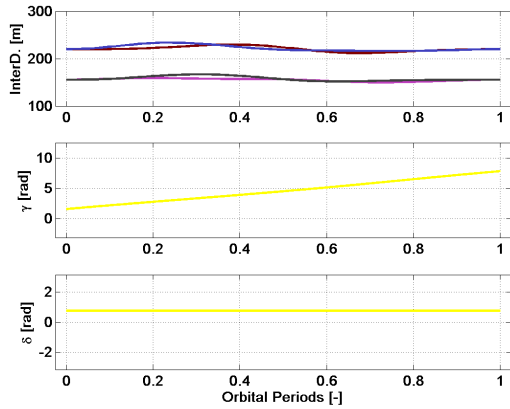
sideration is:

$$J = \int_{t_i}^{t_f} \sigma dt. \quad (43)$$

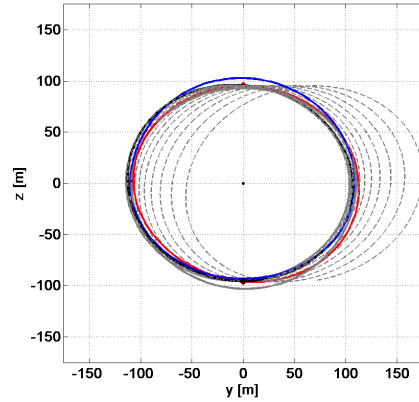
Moreover, both control authorities described previously have been considered also for the multiple femto-spacecraft scenario, i.e. spacecraft are assumed with full and limited control capabilities.

## 7. Conclusion

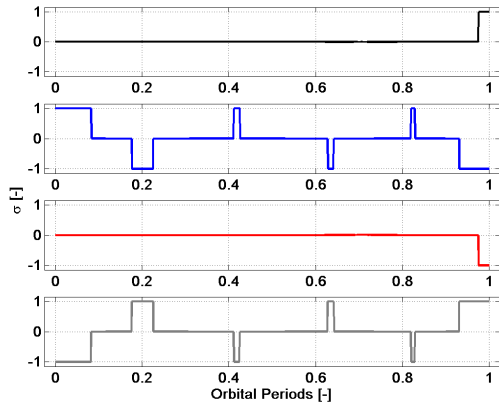
An optimal control problem formulation has been presented in this paper to investigate reconfiguration and maintenance maneuvers for relative motion. The exact  $J_2$  nonlinear relative dynamics has been considered and a complex scenario has been investigated: change of the orbital relative amplitude and shift of the formation-flying centre at the same time. Two femto-spacecraft have been considered for a sake of clarity, but the approach can be easily extended to many more ele-



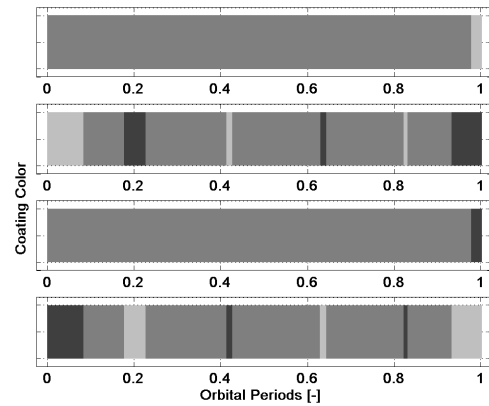
(a) Femto-spacecraft inter-distance and control directions.



(b) Reconfiguration maneuver,  $y-z$  plane view.



(c) Control magnitude  $\sigma$ .



(d) Differential coating color.

Figure 18. Reconfiguration maneuver (Case 1) for limited control capability multiple femto-spacecraft scenario: relative motion and control magnitude.

ments. Different control authorities have been considered: femto-spacecraft with full and limited control capability. The control method reveals to be propellant-free, as it exploits the differential natural perturbation acting on the system, in detail solar radiation pressure.

## Acknowledgements

This research was performed in the framework of the project supported by the European Research Council Advanced Investigator Grant – 227571: VISIONSPACE, Orbital Dynamics at Extremes of Spacecraft Length-Scale.

## 8. References

[1] Atchison, J. A. and Peck, M. “A Millimeter-Scale Lorentz-Propelled Spacecraft.” “Proceedings of the AIAA Guidance, Navigation, and Control Conference,” Vol. 5. 2007.

- [2] Hamilton, D. P. and Krivov, A. V. "Circumplanetary Dust Dynamics: Effects of Solar Gravity, Radiation Pressure, Planetary Oblateness, and Electromagnetism." *Icarus*, Vol. 123, No. 2, pp. 503–523, 1996.
- [3] Lucking, C., Colombo, C., and McInnes, C. R. "Electrochromic Orbit Control for Smart-Dust Devices." *Journal of Guidance, Control, and Dynamics*, Vol. 35, 2012.
- [4] Xu, S. and Wang, D. "Nonlinear Dynamic Equations of Satellite Relative Motion Around an Oblate Earth." *Journal of Guidance, Control, and Dynamics*, Vol. 31, No. 5, 2008.
- [5] Vallado, D. *Fundamentals of Astrodynamics and Application*. Kluwer Academic Publishers, 2001.
- [6] Vadali, S. R., Schaub, H., and Alfriend, K. T. "Initial Conditions and Fuel-Optimal Control for Formation Flying of Satellites." "Proceedings of the AIAA Guidance, Navigation, and Control Conference," 1999.
- [7] Alfriend, K., Vadali, S. R., Gurfil, P., How, J., and Breger, L. *Spacecraft Formation Flying: Dynamics, Control, and Navigation*, Vol. 2. Butterworth-Heinemann, 2009.
- [8] Bryson, A. E. and Ho, Y. C. *Applied Optimal Control*. Wiley, New York, 1975.
- [9] Atchison, J. A. and Peck, M. "A Passive, Sun-Pointing, Millimeter-Scale Solar Sail." *Acta Astronautica*, Vol. 67, No. 1-2, pp. 108–121, 2010.
- [10] Schaub, H. and Alfriend, K. T. "J2 Invariant Relative Orbits for Spacecraft Formations." *Celestial Mechanics and Dynamical Astronomy*, Vol. 79, No. 2, pp. 77–95, 2001.